

pubs.acs.org/acscatalysis Research Article

Pretreatment Effects on the Surface Chemistry of Small Oxygenates on Molybdenum Trioxide

Sean Najmi,[#] Mathew Rasmussen,[#] Giada Innocenti, Chaoyi Chang, Eli Stavitski, Simon R. Bare, Andrew J. Medford,^{*} J. Will Medlin,^{*} and Carsten Sievers^{*}



Cite This: ACS Catal. 2020, 10, 8187–8200



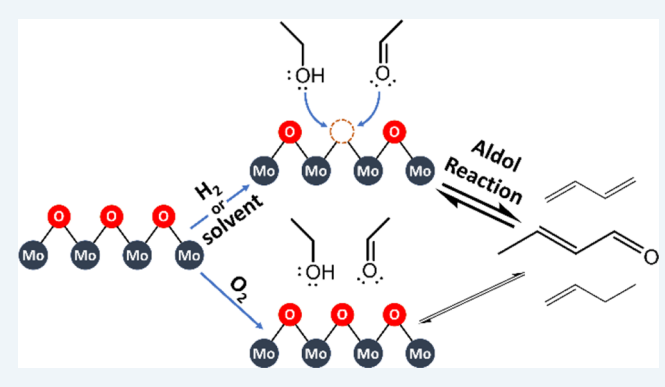
ACCESS

III Metrics & More

Article Recommendations

s Supporting Information

ABSTRACT: Understanding surface reactions of biomass-derived oxygenates on metal oxides is important for designing catalysts for valorization of biomass. This work elucidated the effect of different pretreatments on molybdenum trioxide (MoO₃) to understand how surface reactivity is controlled by the surface oxidation state. The catalyst was pretreated in oxidative, inert, and reducing environments. The inert and reducing pretreatments created oxygen vacancies on the catalyst surface that acted as active sites for the adsorption of oxygenated molecules, with the reducing pretreatment yielding a higher density of these active sites. Exposing the catalyst to an alcoholic solvent such as methanol also led to a partial reduction similar to the inert pretreatment. After pretreatment, the catalyst was exposed to ethanol, acetaldehyde,



and crotonaldehyde with subsequent characterization by diffuse reflectance infrared spectroscopy (DRIFTS), temperature-programmed desorption (TPD), X-ray absorption near edge spectroscopy (XANES), and X-ray photoelectron spectroscopy (XPS). Density functional theory (DFT) was also used to determine adsorption configurations and energies of ethanol, acetaldehyde, and crotonaldehyde. Reduced surfaces were shown to have a stronger affinity for carbonyls, leading to a higher activity for the aldol condensation of acetaldehyde and ethanol to C_4 molecules. Catalysts pretreated in an oxidative environment were completely inactive toward chemisorption and reaction of acetaldehyde.

KEYWORDS: molybdenum oxides, aldol condensation, alcohol oxidation, reducible oxides, Lewis acid

1. INTRODUCTION

Developing processes for producing oxygen-containing commodity chemicals from biomass has garnered considerable attention. Biomass-derived sugars have the potential to revolutionize the way chemicals, such as lactic acid and ethylene glycol, are produced by offering a more efficient pathway compared to conventional processes. ^{1–4} The design of heterogeneous catalysts that promote selective transformations of sugars remains a major challenge. ⁵

Solid catalysts containing Lewis acid sites have shown promise for many desired reactions of sugars, including isomerization, retro-aldol condensation and the Cannizzaro reaction. These sites can accept electrons and therefore activate reactant molecules. Several descriptors, such as hardness, electronegativity, and ionic radii, have been proposed to better characterize the nature of Lewis acid properties in different materials. However, the influence of these factors on catalytic activity and selectivity remains only partly understood. One solid Lewis acid catalyst, tin-containing zeolite Beta (Sn-BEA), was shown by Davis and co-workers to isomerize glucose to fructose through a 1,2-intramolecular hydride shift in the presence of water as the solvent, but this

catalyst showed limited activity for the desired subsequent retro-aldol condensation (RAC). The Sn sites in the zeolite are isolated Lewis acid sites that hypothetically bond with the α -hydroxyl group of glucose and then transfer the hydrogen to the carbonyl group to become fructose. In contrast, molybdenum(VI) trioxide (MoO₃) is an effective catalyst for RAC of fructose to dihydroxyacetone (DHA) and glyceraldehyde (GLA), which could then be converted to alkyl lactates. They also found that the overall carbon yield increased when ethanol was used as a solvent rather than water under the same conditions with MoO₃. However, the nature of the active sites on molybdenum oxide and the origins for their high retro-aldol activity remain unknown.

Recently, density functional theory (DFT) was employed to calculate the thermodynamics and kinetics of reactions

Received: May 4, 2020 Revised: June 29, 2020 Published: June 30, 2020





involving MoO₃. Rellán-Piñerio and López studied the Formox process (methanol oxidation to formaldehyde) with DFT calculations and found that Mo(VI) cycles to Mo(IV) during reaction, with oxygen vacancy formation being a key step in the catalytic cycle. 13 Vlachos and co-workers used DFT to obtain the free energy profile of the retro-aldol fragmentation of fructose to DHA and GLA.¹⁴ They proposed a monodentate intermediate, in which the oxygen atom of the carbonyl group binds to a single Mo(VI) site. López and co-workers also used DFT to describe the epimerization of glucose to mannose on both a fully oxidized and defective MoO₃ surface. These modeling studies provide additional atomic-scale predictions of the nature of the active site on MoO3, but additional confirmation regarding the behavior MoO3 under relevant conditions through in situ and/or operando experiments is currently lacking.

In addition to being an important solvent for sugar chemistry and other biomass transformations, ethanol has been extensively studied as a feedstock for biorefineries due to well-established processes for its production, its cheap cost, and ease of implementation into current technologies. 16-18 Moreover, ethanol is a useful probe molecule for studying aldol processes on metal oxide surfaces. 19 One such aldol reaction, known as the Lebedev process, transforms ethanol into 1,3butadiene, a valuable chemical for rubber production.²⁰ It was recently shown that there is an optimal density of Lewis acid sites for the selective reaction to butadiene. 21,22 Another example of aldol condensation, the Guerbet reaction, converts primary alcohols to longer chain alcohols, which can often be used as fuel additives.²³ For example, Barta and co-workers² found that nickel- and copper-doped porous metal oxide catalysts were able to transform ethanol to butanol with significant yields. These important developments make ethanol an attractive reactant for further study and highlight the role of Lewis acid sites on the conversion of ethanol.

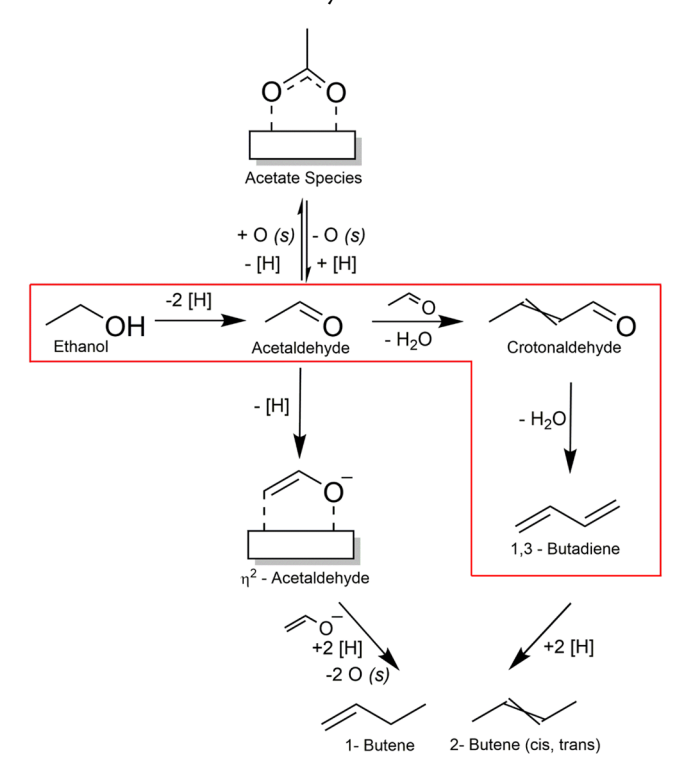
In this work, the effect of reduction during typical thermal pretreatments of MoO_3 in H_2 , N_2 , and O_2 and their consequences for aldol reactions were studied. Adsorption and reactions of the probe compounds ethanol, acetaldehyde, and crotonaldehyde were analyzed and discussed considering the nature of active sites during reaction conditions (see Scheme 1). The effect of alcoholic solvents as a reducing agent to the surface of MoO_3 is also investigated.

2. METHODS

2.1. Materials. Commercial MoO $_3$ (\geq 99.5%, Sigma-Aldrich) was calcined in dry air at 450 °C for 4 h and utilized for all experiments. Pretreatment gases included H $_2$ (99.999%, Airgas), He (99.999%, Airgas), and O $_2$ (99.994%, Airgas). Ethanol (\geq 99.5%), acetaldehyde (\geq 99.5%), crotonaldehyde (\geq 99%, predominately trans) and potassium bromide (\geq 99.0%), were purchased from Sigma-Aldrich for FTIR experiments. For TPD experiments, ethanol (200 Proof, Decon Laboratories), acetaldehyde (99.5%, Acros Organics), crotonaldehyde (\geq 99% predominately trans, Sigma-Aldrich), 1,3-butadiene (\geq 99%, Sigma-Aldrich) and 1-butene (\geq 99%, Sigma-Aldrich) were used.

2.2. Catalyst Characterization. 2.2.1. N₂ Physisorption. A Micromeritics Accelerated Surface Area and Porosity (ASAP) 2020 system was used for N₂ physisorption followed by BET analysis. ²⁶ Before analysis, samples were degassed at 110 °C and held at this temperature for 4 h. Adsorption–desorption measurements of nitrogen were carried out at –196

Scheme 1. Reaction Pathways for Conversion of Ethanol^a



^aThe boxed route is Toussaint's mechanism of aldol condensation. ²⁵.

 $^{\circ}$ C. After being calcined in air at 450 $^{\circ}$ C for 4 h in air, the sample was sieved >90 μ m and one gram was used for the experiment.

2.2.2. XRD. Powder XRD (X-ray Diffraction) patterns were measured on a Philips X'pert diffractometer equipped with an X'celerator module. Diffractograms were obtained with Cu $K\alpha$ radiation for $2\theta = 10-80^{\circ}$ with a step size of 0.0167° . In situ X-ray diffraction data were collected at the Quick Absorption and Scattering beamline (QAS, 7-BM) at the National Synchrotron Light Source II (NSLS-II). The samples were placed in the Clausen cell and hydrogen was flowed through the glass at the rate of 20 sccm. The patterns were collected using 19 keV photons with PerkinElmer flat panel detector. The energy was calibrated using a LaB₆ standard, and the 2D patterns were integrated using Dioptas software.

2.3. XANES. Mo L₃-edge X-ray absorption near edge spectroscopy (XANES) experiments were performed at beamline 4-3 at the Stanford Synchrotron Radiation Laboratory (SSRL). The Si(111) monochromator was calibrated by setting the edge energy of a Mo foil reference to a standard value of 2520.0 eV. For the in situ experiments, the Mo L₃ edge was analyzed in fluorescence mode using a passivated implanted planar silicon (PIPS) detector. The sample was prepared by diluting MoO3 with BN to create a mixture with roughly 11 wt % MoO₃. This mixture was packed into a sample holder and placed in a specially designed cube reactor cell 27 for analysis. XANES of the Mo L_3 edge was collected continuously during a series of treatments performed consecutively on the same sample. First, the sample was heated at 10 °C/min in 40 sccm He from room temperature to 450 °C and held at that temperature for 30 min. The sample was then cooled to room temperature, and the flow was switched to 40 sccm of 10% H₂ in He. The sample was then heated at 10 ACS Catalysis pubs.acs.org/acscatalysis Research Article

 $^{\circ}$ C/min from room temperature to 450 $^{\circ}$ C for 30 min. Subsequently, the sample was cooled to 350 $^{\circ}$ C, and the flow was switched to 40 sccm O_2 and held at this temperature for 30 min before cooling down to room temperature again in 40 sccm He. The XANES data were processed using Athena.

To understand catalyst changes due to solvent effects, X-ray absorption spectra were recorded at the National Synchrotron Light Source II (NSLS-II) (Brookhaven National Laboratory, NY, U.S.A.) at a damping wiggler/Inner Shell Spectroscopy beamline using a cryogenically cooled double crystal Si(111) monochromator. The beam spot on the sample was 0.9×0.9 mm². The X-ray absorption near-edge structure (XANES) spectra was recorded at the Mo K-edge (20000 eV) in transmission geometry mode using ion chambers as detectors. Spectra were acquired at room temperature using self-supporting pellets of the catalyst powder mixed with boron nitride.

2.4. XPS. XPS experiments were carried out in a Multiprobe ultrahigh vacuum (UHV) system with a base pressure $<5 \times 10^{-10}$ Torr, equipped with a hemispherical electron energy analyzer (SPECS, PHOIBOS 100) and a twin anode X-ray source (SPECS, XR50). The XPS spectra were fitted using the add-on function XPST in Igor. Due to spin orbit coupling, the ratio between the Mo $3d_{5/2}$ and Mo $3d_{3/2}$ peaks was constrained to 3/2. Because only a partial reduction was expected, the fit was performed assuming no Mo(IV) was present in the sample. The locations and widths of the peaks were constrained based on literature values compiled elsewhere, ²⁹ and the areas of these peaks were fit based on these parameters.

2.5. DFT Calculations. A model surface based on the (100) facet of α -MoO₃ (space group *Pnma*) was selected as the most stable bulk structure and surface facet. 13-15 All density functional calculations were performed with Quantum ESPRESSO, 30 and exchange-correlation interactions were treated with the BEEF-vdW functional.³¹ The BEEF-vdw functional is parametrized for surface adsorption and does not require material-specific parameters, so we elected to use it instead of the + U correction. There are numerous studies of MoO_3 with 32,33 and without + U, 14 and there is no consensus on its necessity for adsorption properties or the appropriate U value, 33,34 so the correction was omitted for simplicity. A Monkhorst-Pack k-point sampling of $5 \times 5 \times 1$ with a planewave cutoff of 450 eV was used for all MoO_3 calculations. A Fermi-Dirac electron smearing width of 0.1 eV was used for convergence (results extrapolated to 0 K) with spin polarization and dipole correction.³⁶ The slab was modeled using 20 Å of vacuum between slabs, and the lower two layers were fixed to bulk positions. The L-BFGS algorithm implemented in the Atomic Simulation Environment (ASE)³ was applied for geometry optimization (maximum force of 0.05 eV/Å). The adsorption energies were calculated as follows:

$$E = E_{\rm slab+ads} - E_{\rm slab} - E_{\rm ads}$$

where E is the adsorption energy with $E_{\rm slab+ads}$, $E_{\rm slab}$, and $E_{\rm ads}$ as the DFT energy of the adsorption complex, slab, and adsorbate, respectively. Free energies were computed in a similar way, with Gibbs free energies used in place of DFT energies.

Vibrational modes were estimated with the normal-mode analysis by using a finite difference approximation of the Hessian matrix ($\Delta r = 0.01$ Å) using ASE. Free energies were computed using the ideal gas approximation for gas-phase

species and the harmonic approximation for adsorbates. A temperature of 300 K and a pressure of 1 bar were used in the free energy calculations. These corrections were also computed with the thermochemistry package of ASE, and a low-frequency cutoff of 50 cm⁻¹ was used for adsorbed species.³⁸ Initial guesses for adsorbate geometry and binding site were based on structures from previously reported DFT calculations.¹³

2.6. In Situ DRIFTS Studies. DRIFTS spectra were collected using a Nicolet 8700 FT-IR equipped with a liquid nitrogen cooled MCT/A detector and the Praying Mantis (Harrick Scientific) accessory with a high temperature reactor for in situ studies. Spectra were averaged at 64 scans with a resolution of 4 cm⁻¹. All spectra were treated using the Thermo Scientific Omnic Software. A background of dried potassium bromide at 50 °C was used for all spectra. The sampling cup was filled with catalyst and then smoothed across several times to ensure an even layer. The reactor was sealed and flushed with 100 sccm N₂ for 5 min to settle the sample bed. Additional catalyst powder was added to fill any voids. The catalyst was pretreated in 40 sccm of H₂, N₂ or O₂ for 1 h at 450 °C at a ramp rate of 10 °C/min and then cooled in an N₂ atmosphere for 1 h to bring the temperature of the sample back to 50 °C. An initial spectrum of the catalyst was collected at this temperature for spectral subtraction against the catalyst with species adsorbed. Ethanol was bubbled in 40 sccm of N₂ for 3 min, acetaldehyde in 5 sccm of N2 for 1 min, and crotonaldehyde in 10 sccm of N2 for 1 min. All probe molecules were introduced to the catalyst bed at 50 °C. After introducing the probe molecule, the feed was switched to 40 sccm of N₂ and held at 50 °C for 30 min and then ramped to 100, 150, and 200 °C at 10 °C/min and held at those temperatures for 30 min. All the spectra were collected at 50 °C after the sample had been heated to the respective reaction temperature.

2.7. TPD Studies. For each experiment, about 500 mg of MoO_3 was loaded into a quartz reactor tube, and quartz wool was added to the ends of the catalyst bed. Samples were pretreated in a flow of 36 sccm of either H_2 or He at 450 °C for 1 h. After cooling the sample down to room temperature, probe molecules were dosed on the surface by flowing 9 sccm of He through a bubbler containing the desired compound and then over the catalyst bed for 80 min. The bubbler was kept at room temperature when dosing ethanol and crotonaldehyde but was cooled to 10 °C for acetaldehyde. Following dosing, the reactor tube was purged with a 9 sccm flow of He for approximately 8 h. After purging, the temperature was ramped from room temperature to 715 °C at a heating rate of 10 °C/min. FDesorbed products were detected using a Pfeiffer Prisma quadrupole mass spectrometer downstream of the reactor.

Calibration curves were generated to correlate mass spectrum peak areas to molar amounts for each reactant/product. Controlled volumes of each molecule were injected into the mass spectrometer while monitoring the peak response. Desorption product signals were normalized using the calibration curves according to the following characteristic fragments: ethanol (m/z=31), acetaldehyde (m/z=29), 1,3-butadiene (m/z=54), 1-butene (m/z=56), and crotonaldehyde (m/z=70). For masses associated with multiple products, molecular desorption rates were deconvoluted by subtracting contributions of heavier products using mass fragmentation patterns obtained on our system. Total molar quantities of each desorption product were calculated by

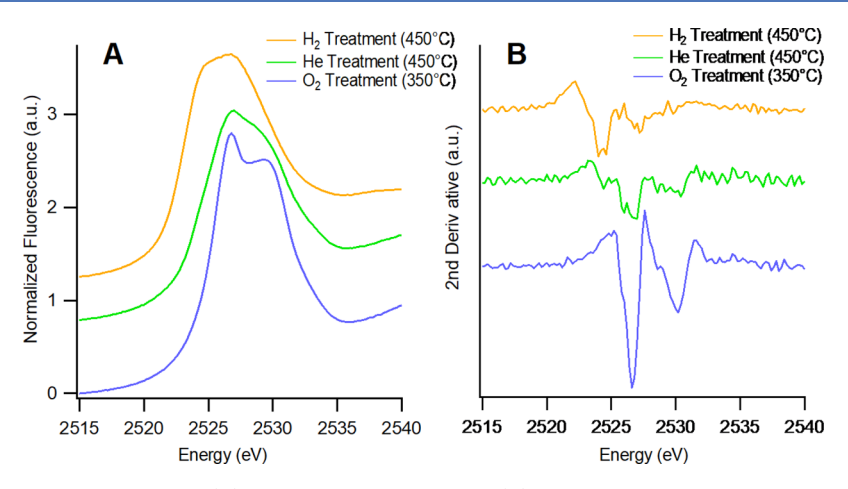


Figure 1. Normalized Mo L3 edge XANES data (A) and the second derivative (B) for MoO3 after treatment with O2, He, and H2

integrating the normalized spectra of the relevant characteristic mass fragment with respect to time.

3. RESULTS

3.1. Catalyst Pretreatments and Characterization. Samples reduced in H₂ are noted as R-MoO_x, samples exposed to an inert gas (either N2 or He) are noted as I-MoO_x, and samples pretreated with oxygen are noted as O-MoO₃. XRD showed that only orthorhombic MoO₃ was present before and after calcination of MoO₃ for 4 h in air (Figure S1 of the Supporting Information, SI). Peak locations were shifted slightly after calcination, and the d spacing of the crystals decreased (Table S1). This was most likely due to the removal of water during calcination. In-situ XRD showed that at higher temperatures in the presence of hydrogen, the bulk crystal structure of the catalyst did not change (Figure S1B). The surface area of the catalyst was below 2 m²/g according to N₂ physisorption. Delporte reported that as extent of reduction increases, the surface area of MoO₃ increased from 4 m²/g to 11 m²/g.³⁹ Thus, a higher surface area is a possible contributor to enhanced rates of product formation on reduced samples.

The evolution of the color of MoO, during the pretreatment gave a first indication of its oxidation state. Heating in an oxygen flow produced no noticeable color change up to 450 °C. Heating in inert flow caused the sample to turn slightly blue at around 250 °C, which continued to intensify up to the final temperature of 450 °C indicating progressive reduction. In hydrogen flow, the sample turned a dark violet shade similar to MoO₂.

The Mo L₃ edge structure is derived primarily from the transition of core electrons in the 2p_{3/2} orbital to empty 4d orbitals. However, these vacant d orbitals can be split into e_g and t_{2g} states due to ligand interactions in octahedrally coordinated molybdenum oxides. This crystal field splitting causes a doublet peak shape in the white line, as seen clearly in the MoO₃ sample after O₂ treatment (Figure 1A). Differences in the splitting energy can be seen more clearly by plotting the second derivative of the signal intensity (Figure 1B).⁴⁹ Local minima in this plot correspond to peak maxima in the fluorescence data. Another key feature of the XANES spectra, the absorption edge energy, is often interpreted as the first inflection point in the white line. This edge energy is expected to move to lower energy with decreasing oxidation state. 44,50,51 The shape and position of the edge are also influenced by the symmetry of the coordination

sphere around the absorbing atom. 52,53 The absorption edge energy along with the splitting energy difference for the MoO₃ sample after each treatment are compiled in Table 1.

Table 1. Mo L₃ Edge and Splitting Energies

	edge position (eV)	splitting energy (eV)
O ₂ treatment	2525.6	3.6
He treatment	2524.2	3.4
H ₂ treatment	2523.1	3.2

Following the oxidative treatment, the Mo L₃ edge energy was determined to be 2525.6 eV with a d-orbital splitting difference of 3.6 eV, which is indicative of fully oxidized MoO₃.^{47,54,55} After heating in He, the edge position and splitting energy were shifted downward by 1.4 and 0.2 eV, respectively. The high temperature H₂ treatment had a similar effect on both the edge position and splitting energy shifting them further downward by a similar increment. Previous research demonstrated that decreases in both the splitting energy and edge position of metal oxides tend to correlate with reduction in the oxidation state of the metal ion. 44,50,51 As such, it appears that the He treatment causes a slight reduction in Mo(VI) centers, and this effect is enhanced by high temperature treatment in H₂.

Previously published XANES profiles of MoO₃ and MoO₂ from Kashiwabara et al. were used as standards to obtain relative edge positions of the Mo(VI) and Mo(IV) oxidation states (see Figure S2).41 In this study, the Mo L3 edge was shifted down by 1.4 and 2.5 eV after high temperature exposure to He and H₂ respectively. This compares to a shift of approximately 2.2 eV between MoO₃ and MoO₂ standards (Figure S2). Using the relationship between edge position and oxidation state obtained from the digitized spectra, this may indicate that the He treated sample is slightly reduced to an intermediate oxidation state around Mo(V), while the H₂ treated sample is highly reduced to a Mo(IV) or lower state.

Several groups have shown that the reduction of bulk MoO₃ with hydrogen can result in the formation of hydrogen molybdenum bronzes under mild conditions. 56,57 In this study, the higher ramp rates and reduction temperatures used during pretreatment would likely have suppressed the formation of these structures. Aritani et al. found that the XANES peaks for type I and type II bronzes were shifted to slightly lower energy compared to MoO₃. In contrast, the shifts in peak positions

ACS Catalysis pubs.acs.org/acscatalysis Research Article

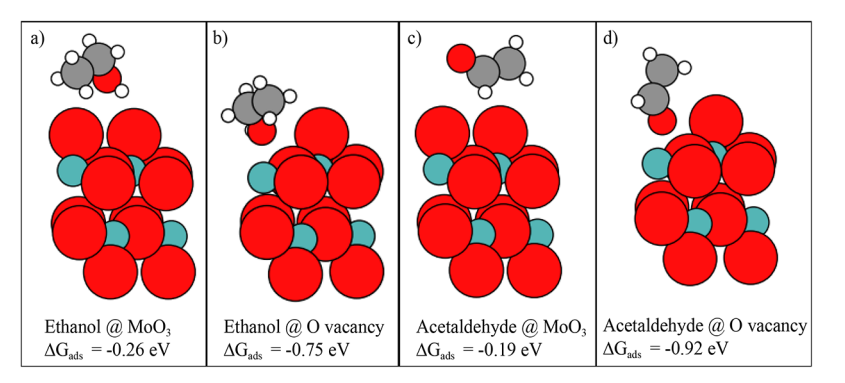


Figure 2. Adsorption geometries of ethanol (a, b) and acetaldehyde (b, c) adsorbed on a pristine MoO₃ (100) surface (a, c) and an oxygen vacancy defect (b, d). The Gibbs free energy of adsorption is included for each system. Mo atoms (teal) and bulk O atoms (red) are represented by their ionic radii, while H (white), C (gray), and O atoms in adsorbates are represented with covalent radii.

seen between MoO_3 and the H_2 treated sample in this study were much larger. In addition, the in situ XRD (Figure S1B) of MoO_3 in H_2 at elevated temperatures does not reveal changes in the original diffractogram that would correspond to the formation of a bronze phase. As such, while there is no evidence to suggest the presence of hydrogen molybdenum bronzes after H_2 treatment, their presence cannot be ruled out.

Changes of the oxidation state of MoO₃ through reactions with methanol were probed by XPS and XANES. When MoO₃ was exposed to methanol and then held under vacuum overnight, the color of the catalyst changed from light green to gray-blue, indicating a reducing interaction between the solvent and the MoO₃ surface. This change was verified through XANES of MoO₃ before and after exposure to methanol at the K-edge as reported in Figure S3. A slight decrease in the near edge peak is seen at 20002 eV. Since this near edge peak does not exist for Mo(IV), ⁵⁸ this result suggests that methanol exposure produced a slight decrease in the average oxidation state of Mo. The fits of the Mo 3d doublet in the XPS spectra before and after exposure to methanol (Figure S4) indicated that the abundance of Mo(V) increased from 8% to 15% during this treatment.

3.2. Reaction of Oxygenates on Different Surfaces. 3.2.1. DFT Calculations. DFT calculations were used to investigate how the presence of oxygen vacancies on MoO3 influences the binding of ethanol and acetaldehyde. The optimized adsorption geometries for ethanol and acetaldehyde on O-MoO₃ indicate only nondirectional bonds and relatively low adsorption energies of roughly -0.20 eV (Figure 2). These results provide evidence that both molecules are physisorbed on O-MoO₃. In contrast, there was a clear directed interaction between the alcohol/aldehyde group and the oxygen vacancy site, and binding energies were substantially more exergonic (<-0.75 eV), indicating strong chemisorption at the vacancy sites. This suggests that defect sites are critical to activating alcohol and aldehyde functionalities and corroborates the enhanced reactivity of partially reduced surfaces described below. Vibrational frequencies are shown in Tables S2-S4 for both types of surfaces and the three adsorbate molecules. For ethanol, the defect site generally induced a slight blueshift of 0-50 cm⁻¹ for most modes, although the O-H stretch is significantly more red-shifted by around 150 cm⁻¹. For acetaldehyde, the effects of the defect site are more ambiguous. Most modes were slightly blue-shifted (0-50 cm⁻¹), while the C-C and C-H stretch of the CH group was red-shifted by 45 and 116 cm⁻¹, respectively.

3.2.2. DRIFTS Studies. DRIFTS was used to further illustrate the role of oxygen vacancies in strong adsorption and conversion of ethanol, acetaldehyde, and crotonaldehyde at ambient conditions and subsequent heating. Figure 3A shows the DRIFTS spectra of ethanol on the three differently pretreated surfaces at 50 °C, and Table 2 gives vibrational assignments for the relevant peaks labeled in Figure 3A. While the relative absorbance for $R-MoO_x$ were less intense, it is likely the reduced intensities were due to a higher infrared absorbance (darker color) of the sample, and not necessarily due to the adsorbate concentration.

The region above 3200 cm⁻¹ is classified as the hydroxyl stretching region. ^{60,61} For the reduced sample, adsorption of ethanol resulted in a broad, unresolved peak at 3331 cm⁻¹. The poor signal-to-noise ratio for this sample is likely due to the stronger IR absorbance (darker color) of prereduced MoO₃. In contrast, the inert and oxidative pretreatments produced samples with several distinct hydroxyl bands. Bands at 1479 and 1447 cm⁻¹ suggested the presence of acetate species on the surface. ^{62,63} Previous studies have shown that acetate species are produced on different metal oxides after ethanol exposure. 63-70 There was a shoulder to the peak marked 1625 cm⁻¹ on the R-MoO_x that appeared around 1645 cm⁻¹. As discussed below, this peak is most likely the v(C=C) mode of crotonaldehyde. Two other bands appeared at 1268 and 1624 cm⁻¹ and are attributed to the v(C-O) and v(C=C)vibrations of surface bound enolates, respectively. These peaks were retained up to 150 °C (Figure S6) suggesting that the enolates are strongly bound. Idriss et al. referred to this species as η^2 -acetaldehyde due to the coordination of both the primary carbon and oxygen atom to the surface (Scheme 1).65,66 The presence of this species suggests that keto-enol tautomerization of surface species readily occurs on the catalyst, similar to what was observed in the case of dehydration products of glycerol on niobia.

The C–H stretches of ethanol gave rise to peaks near 2978, 2935, and 2902 cm⁻¹ that are attributed to $\nu_{\rm as}({\rm CH_3})$, $\nu_{\rm as}({\rm CH_2})$, and $\nu_{\rm s}({\rm CH_2})$ modes, respectively. This suggests that significant amounts of ethanol were still present on the surface as either ethoxide groups or in a molecularly adsorbed state. The C–H stretching modes of surface species on the R–MoO_x sample decreased significantly when the temperature was increased above 50 °C, while they remained resolved on the I–MoO_x sample even at 150 °C. Looking at the OH and CH stretching region, it appears that ethanol adsorbs differently based on the pretreatment for the catalyst given

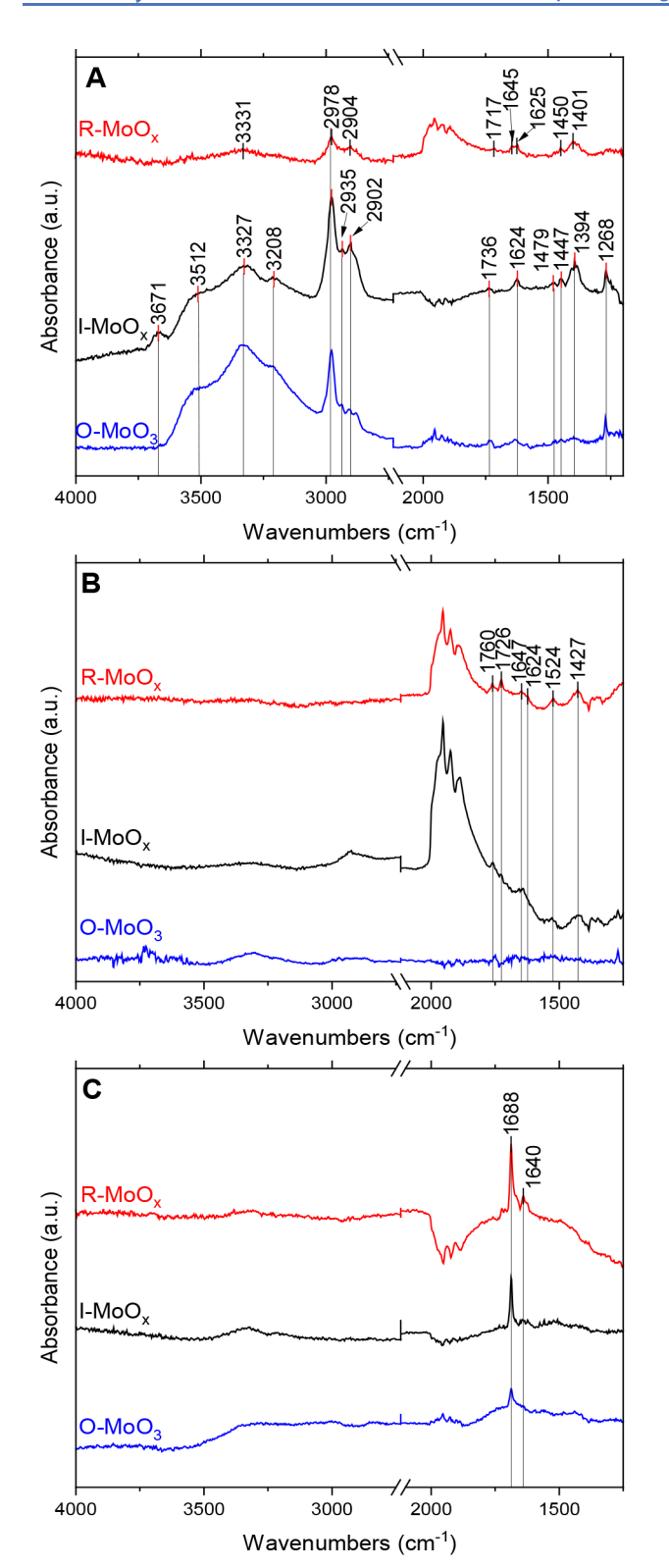


Figure 3. Spectral subtraction DRIFTS of (A) ethanol adsorbed onto R-MoO_x, I-MoO_x, and O-MoO₃ sample at 50 °C. (B) acetaldehyde adsorbed onto R-MoO_x, I-MoO_x, and O-MoO₃ sample at 100 °C. (C) crotonaldehyde adsorbed onto R-MoO_x, I-MoO_x, and O-MoO₃ sample at 100 °C.

more surface hydroxyl groups appear on the $I-MoO_x$ and $O-MoO_3$ surface due to higher presence of oxygen on the surface.

Table 2. Vibrational Mode Assignments from Labeled Peaks in Figure 3A for Species Other than Ethanol

Mode (cm ⁻¹)	Vibration	Species
1268	υ(C-O)	Enol
1393	$\delta_{as}(CH_3)$	Acetaldehyde
1427	δ(CH _x)	Various
1447	$\delta_{as}(CH_3), v_s(COO)$	Various
1479	$\delta_{as}(CH_2)$	Various
1524	vas(COO)	Acetate
1624	v(C=C)	Enol
1645/7	v(C=C)	Crotonaldehyde
1726	υ(C=O)	Acetaldehyde (Chemisorbed)
1735	v(C=O)	Acetaldehyde
1760	v(C=O)	Acetaldehyde (Physisorbed)

Figure 3B shows the spectra of acetaldehyde on the three different pretreated surfaces at 100 °C. One key feature of these spectra is the appearance of Mo=O overtones in the $1800-2000~{\rm cm}^{-1}$ region. The appearance of these overtones suggests a strong interaction between acetaldehyde and the Mo=O bond. The peaks at 1726 and 1760 cm⁻¹ are characteristic of the v(C=O) for chemisorbed and physisorbed acetaldehyde, respectively. The peak at 1524 cm⁻¹ is attributed to surface acetate species. The R-MoO_x sample showed additional peaks. The peak at 1624 cm⁻¹ was the same as the one shown in Figure 3A and is assigned to the v(C=C)of an enol. The peak at 1647 is assigned to the v(C=O) of the aldol coupling product crotonaldehyde.⁷⁴ This peak was also seen in Figure 3A,C. The broad peak at 1427 cm⁻¹ is assigned to $\delta(CH_x)$ modes of various species.⁷⁴ As the temperature increased, the peaks diminished at 200 °C suggesting desorption (Figure S7A). This was also observed for the I-MoO_x sample (Figure S7B). The reduced samples had higher affinity for adsorption of acetaldehyde onto its surface than the O-MoO₃ sample. Interestingly, acetaldehyde only adsorbed very weakly on the O-MoO₃ sample. While there was some physisorbed acetaldehyde present on the surface at 50 °C (Figure S7C), after heating to 100 °C, there were no detectable peaks present.

Figure 3C shows the spectra of crotonaldehyde on the three differently pretreated surfaces at 100 °C. The sharp peak at 1688 cm⁻¹ is assigned to the v(C=O) stretching mode of crotonaldehyde, which was red-shifted from 1725 cm⁻¹ in the gas phase. A shoulder was present around 1640 cm⁻¹ and is assigned to the v(C=C) stretching mode of crotonaldehyde.⁷⁵ The sustained presence of this band up to 200 °C on R-MoO, and I-MoO_r (Figure S8A/B) suggests it was chemisorbed. There were two resolved v(O-H) peaks present at 3215 and 3334 cm⁻¹ that persisted up to 150 °C. As the temperature increased, the peak at 1688 cm⁻¹ decreased in intensity, and positive peaks of the overtones of the catalyst appeared (Figure S8B). This is similar to the behavior of acetaldehyde on the I-MoO_x sample shown in Figure S7B. The spectrum of crotonaldehyde on R-MoOx contained the same peaks, but the overtones gradually decreased as the temperature increased (Figure S8A). The spectrum of crotonaldehyde on O-MoO₃ exhibited the same 1688 cm⁻¹ peak, but it disappeared after 100 °C, unlike acetaldehyde on the MoO₃ sample which lost its carbonyl peak after 50 °C (Figure S7C). This suggests that crotonaldehyde was more strongly adsorbed on the oxidized surface compared to acetaldehyde on the same surface but still readily desorbed.

3.2.3. TPD MS Studies. TPD was used to determine how reduction of MoO₃ influenced product yields and kinetic barriers for reactions of ethanol, acetaldehyde, and crotonaldehyde. During ethanol TPD on the R-MoO_x surface, ethanol

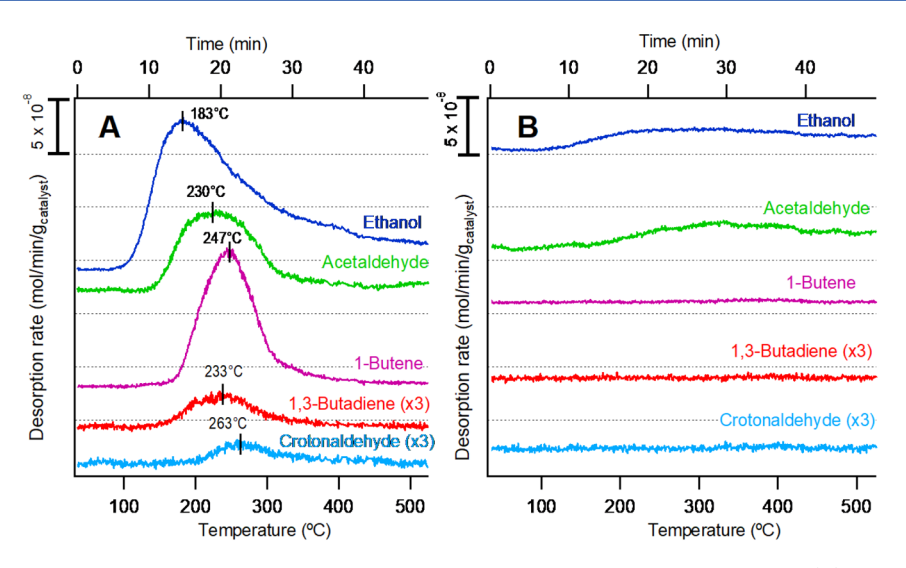


Figure 4. TPD profile of products from ethanol dosed on a MoO₃ surface pretreated with 36 sccm of hydrogen (A) or helium (B) at 450 °C for 1 h. Assignments of each trace are as follows: ethanol (m/z = 31), acetaldehyde (m/z = 29), 1-butene (m/z = 56), 1,3-butadiene (m/z = 54), and crotonaldehyde (m/z = 70). Contributions from heavier products were subtracted from each trace.

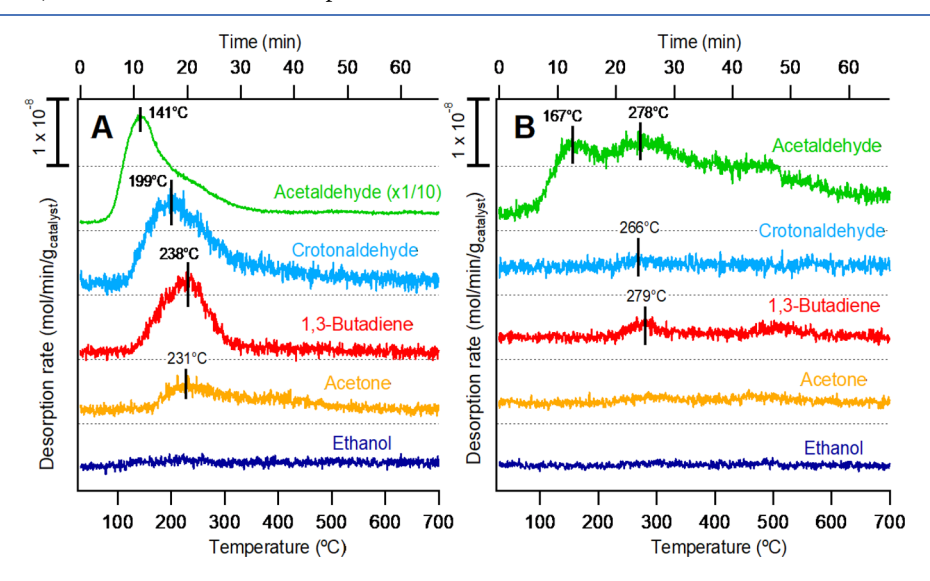


Figure 5. TPD profile of products from acetaldehyde dosed on a MoO₃ surface pretreated with 36 sccm of hydrogen (A) or helium (B) at 450 °C for 1 h. Assignments of each trace are as follows: acetaldehyde (m/z = 29), crotonaldehyde (m/z = 70), 1,3-butadiene (m/z = 54), acetone (m/z = 58), and ethanol (m/z = 31). Contributions from heavier products were subtracted from each trace.

desorbed in a broad, asymmetric peak at 183 °C, while the oxidation product acetaldehyde was formed at 230 °C. Several coupling products were also observed for R-MoO_x, including 1,3-butadiene at 233 °C, 1-butene at 247 °C, and crotonaldehyde at 263 °C. In contrast, the signal for molecular ethanol desorption from the I-MoO_x surface was broad and weak (Figure 4B). A similarly small and broad peak associated with acetaldehyde was also seen on the I-MoO_x surface. The same TPD experiment was also carried out on O-MoO₃, which resulted in lower adsorption and conversion of ethanol. Thus, prereduction of MoO₃ was found to dramatically increase both the density of strong adsorption sites for ethanol and the yield for coupling products. It is worth noting that 1butene may readily isomerize on the oxide surface, and it is likely that the signal attributed to 1-butene also contains contributions from 2-butenes (cis and trans).

The reactions of acetaldehyde were also examined on MoO₃ to better understand the reaction pathway for the production

of C₄ species. On R-MoO_x, a large molecular acetaldehyde desorption peak was observed at 141 °C (Figure 5A). Acetaldehyde was detected at a lower temperature here compared to the ethanol TPD, indicating that the kinetic barrier for producing acetaldehyde from ethanol is higher than the barrier for desorption of molecular acetaldehyde. In other words, the production of acetaldehyde from ethanol is reaction-limited. As expected, coupling products were also observed, with desorption of crotonaldehyde at 199 °C, 1,3butadiene at 238 °C, and acetone at 231 °C. Although similar products were observed for the I-MoO_x surface, their yields were significantly lower, and the peak desorption temperatures (266 and 279 °C for crotonaldehyde and 1,3-butadiene, respectively) were higher. Desorption yields of acetaldehyde were also significantly lower for I-MoO₃. Again, these results indicate that MoO3 reduction greatly increases the density of sites able to activate acetaldehyde toward coupling reactions.

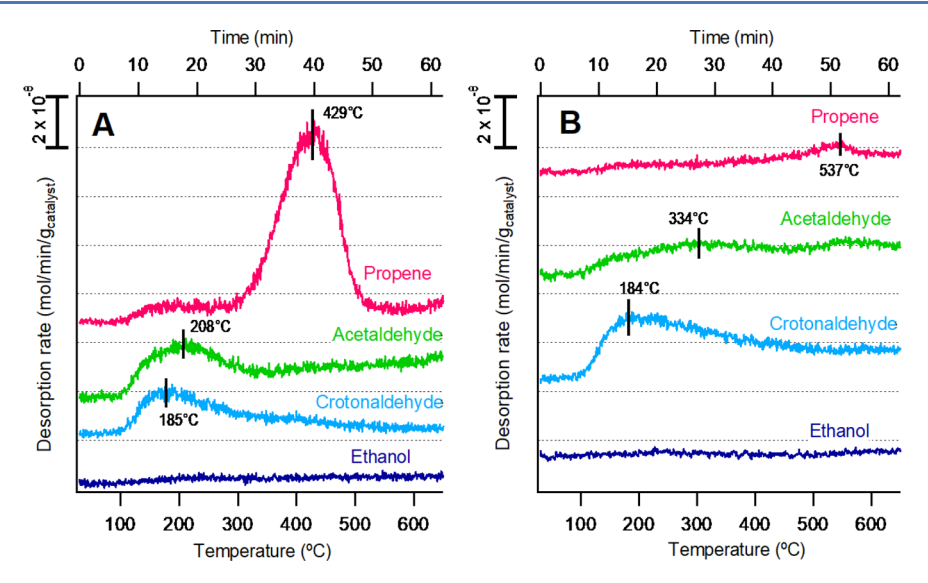


Figure 6. TPD profile of products from crotonaldehyde dosed on a MoO₃ surface pretreated with 36 sccm of hydrogen (A) or helium (B) at 450 °C for 1 h. Assignments of each trace are as follows: acetaldehyde (m/z = 29), ethanol (m/z = 31), propene (m/z = 42), and crotonaldehyde (m/z = 70). Contributions from heavier products were subtracted from each trace.

A noteworthy difference between the acetaldehyde and ethanol TPD data was the relative concentrations of unsaturated C₄ products (1-butene and 1,3-butadiene). When starting with ethanol, R-MoO_x produced a higher concentration of the more saturated 1-butene when compared to 1,3-butadiene. However, when acetaldehyde was used under the same conditions, the C₄ hydrocarbon product contained almost exclusively 1,3-butadiene. This difference in product selectivity may be caused by the difference in the amount of hydrogen available on the surface. When ethanol is coupled to produce C₄ products, hydrogen is removed through dehydrogenation. The resulting hydrogen may remain on the surface, potentially in the form of surface hydroxyls, and ultimately lead to the production of more saturated species like 1-butene. However, acetaldehyde does not produce hydrogen during the coupling to C₄ products, so unsaturated species like 1,3butadiene are presumably more common.

To understand how surface reduction influences retro-aldol reactions, TPD studies with crotonaldehyde as a reactant were carried out (Figure 6). The peak of crotonaldehyde molecular desorption was similarly broad for both R-MoO_r and I-MoO_x. In contrast, the desorption profile for the RAC product acetaldehyde showed drastically different behavior for the two treatments. On the I-MoOx catalyst, the desorption of acetaldehyde from the surface occurred over a broad temperature range, without a clearly resolved desorption peak. However, on the R-MoO_x catalyst, acetaldehyde desorbed with a much sharper and more intense peak at the relatively low temperature of 208 °C. This difference most likely indicates that the R-MoO_x surface had a higher concentration of sites that are efficient for RAC at lower temperature. This could also be due to a higher concentration of water on the surface from the reduction step since hydration of crotonaldehyde is a prerequisite for C-C bond cleavage by RAC. It was also found that the R-MoO_x sample catalyzed decarbonylation to produce large amounts of propene at higher temperatures, while the I-MoO_x sample was not particularly active for this reaction pathway. Decarbonylation of crotonaldehyde is often reported as a mechanism for the deactivation of transition metal catalysts 76-78 and is likely

catalyzed by the irreversible adsorption of the aldehyde group and subsequent decomposition on reduced Mo sites that are readily available on the $R-MoO_x$ surface.

The integrated total molar desorption quantities for each reaction product in the TPD studies are displayed in Tables S5 (ethanol), S6 (acetaldehyde), and S7 (crotonaldehyde). In all cases, the total moles of desorbed species from R-MoO_x surface was at least twice as high (and in many cases far higher) as that from the I-MoO_x surface. In summary, the cumulative TPD results suggest that the H2 reduction treatment had two key effects. First, it greatly increased the density of active sites for the various reactions; as discussed in detail below, we propose that these sites are oxygen vacancies generated during reduction. Second, the reduction treatment decreased the peak temperatures for formation of most products (e.g., acetaldehyde from ethanol), indicating that the generated sites were also more active. We propose that this higher activity is due to an increased Lewis acidity of Mo at greater extents of reduction.

4. DISCUSSION

4.1. Nature of Active Sites. Many studies have shown that oxidation state and reducibility play a key role in the reactivity of metal oxide catalysts. 79,80 Several groups have hypothesized that the active sites for important reactions on metal oxides are oxygen vacancies, due to their ability to exhibit both Lewis acidic and redox properties.81-84 This behavior allows them to facilitate the adsorption and reaction of molecules for a wide range of reactions, from hydrodeoxygenation (on CeO₂, MoO₃, and ZnO)^{85–87} to aldehyde coupling (on CeO₂)^{88,89} and retro aldol condensation.^{7,90} Thus, it is critical to properly account for formation and loss of active sites when the catalyst is exposed to pretreatment and reaction conditions. This study shows that oxygen vacancies are formed on MoO3 at elevated temperatures under inert conditions and, to a much greater extent, under reducing conditions. These reducing conditions are comparable to previous studies of oxygen vacancy formation on MoO_3 86,91,92 Delporte et al. showed that MoO₃ forms a MoO₂ phase under an n-hexane/H2 flow at 350 °C for 3 h, as revealed by XRD,

Figure 7. Potential mechanism for formation of oxygen vacancies on MoO₃ via hydrogen treatment and the stabilization of the ethoxide ion on the surface.

and also that a significant increase in surface area occurred.³⁹ In the present study, XANES in combination with the low surface area of MoO3 suggested that the partial reduction of MoO₃ must extend into the bulk under inert and reducing conditions, because there are not enough surface sites to account for the reduced average oxidation state of Mo. This increase in the density of reduced sites on the surface is likely responsible for the increased activity of the R-MoO, catalyst compared to the I-MoO_x catalyst, as seen in the TPD studies (Figures 4,5, and 6). Additionally, probe reactant molecules appear to interact more strongly with these oxygen vacancy sites than on the pristine catalyst. DFT calculations show the adsorption energy of these molecules is lower on the surface with the defect suggesting they are chemisorbed. Although this calculation was only done for the (100) surface, this trend is hypothesized to translate to other facets. DRIFTS of acetaldehyde (Figure S7A) exhibited overtone peaks on R-MoO_x which could imply that the oxygen atom of the acetaldehyde coordinated to the vacancy site. As a result, new Mo=O bonds are formed that were not initially present after reduction. However, these overtones were not observed on the O-MoO₃ sample, suggesting that the different pretreatments affect how adsorbates interact with the surface. The strength of these oxygen vacancy sites also likely plays a role in the activity and selectivity of the catalyst. According to the Sabatier principle, an optimal catalyst requires a balance between the adsorption/activation of the reactant and the ability to desorb products. Volcano plots relating catalytic activity to a descriptive parameter have been demonstrated for a wide variety of reactions. 93,94 While this type of relationship was not observed in this study, it is possible that further reducing the catalyst could lead to excessive coking of the surface from irreversibly adsorbed products. As such, the presence of an optimal density of oxygen vacancy sites for the aldol reaction requires further research.

Interestingly, alcoholic solvents, such as methanol and ethanol, that are commonly used in liquid-phase reactions can also partially reduce and thus activate MoO₃ catalysts for the RAC reaction under mild conditions.⁷ In this study, XPS (Figure S4) and Mo K-edge XANES (Figure S3) both indicated that exposure of MoO₃ to methanol at room temperature resulted in slight reduction, presumably leading to oxygen vacancies on the surface. This also caused a characteristic color change when the solvents were mixed with the powder. While the mechanism for this reduction is not well-studied in the literature, the deprotonation of these alcohols can cause a higher concentration of protons on the surface, which may lead to an increase in the number of

hydroxyls at the surface. Adjacent hydroxyls may then interact to form a water molecule that leaves and a vacancy site. Partial reduction of the surface during reactions in alcoholic solvents could generate active sites for the aldol reaction and thus have a profound impact on catalytic processes. Efforts to rationally improve processes employing these solvents should account for the ability to produce active centers via chemical reduction even in the absence of strong reductants like H₂.

4.2. Reactions of Oxygenates on Different Surfaces. Several metal oxides adsorb ethanol through deprotonating the alcohol group creating ethoxide groups on the catalyst surface. 62,65,67,69,95–97 On MoO₃, coordinatively unsaturated sites (CUS) in the form of anion-cation pairs at the apical oxygen location (M=O) in the MoO₃ lattice have been hypothesized to stabilize the dissociative adsorption of ethanol into a proton and an ethoxide ion on the surface, as depicted in Figure 7. 98-101 This adsorption state is necessary to further dehydrogenate the ethoxide to acetaldehyde through an α -hydride elimination. Several groups have demonstrated that the mechanism for the production of C₄ products from ethanol proceeds through a dehydrogenation to acetaldehyde followed by an aldol coupling reaction. 22,103-105 The promoting effect of the reducing pretreatment most likely derives from an increase in the density of oxygen vacancies at the surface. The specific mechanism for oxygen vacancy formation under hydrogen flow is not clear, but it may occur through hydroxylation and dehydration of surface terminal M=O bonds.1

Similar to ethanol, acetaldehyde adsorption is likely assisted by CUS sites but to an even greater extent. Other reduced metal oxides have also shown the necessity of CUS sites for acetaldehyde adsorption. 66,74,107-111 High coverage of acetaldehyde and proximity between surface species is important for bimolecular reactions, such as aldol coupling, to occur. Adsorption of acetaldehyde is much stronger when a defect is present as shown by DFT (Figure 2). As shown in Figures 4 and 5, there is appreciable production of crotonaldehyde from both ethanol and acetaldehyde on the R-MoO_x and I-MoO_x samples. A reduced MoO₃ state is critical for the forward and reverse aldol condensation reaction. TPD results demonstrated that R-MoO_x was better able to bind and couple both ethanol and acetaldehyde to C4 products compared to I-MoOx and O-MoO₃. R-MoO_x facilitated the RAC of crotonaldehyde to acetaldehyde at low temperature, while I-MoO_r did not. Thus, it is suggested that stabilization of both product molecules of the retro-aldol condensation by defects is critical for the reaction to occur effectively. Similarly, the IR spectra indicated that acetaldehyde chemisorbs and reacts on R-

Scheme 2. Potential Reaction Mechanism Starting from Ethanol with Desorption Temperatures Based on Adsorption on R-MoO_v Surface (Figure 4A)

MoO_x up to 200 °C (Figure S7A), but only adsorbs weakly on O–MoO₃ with complete desorption occurring after 50 °C (Figure S7B).

In parallel with the coupling route, other species were observed. Acetate intermediates were also present on the surface and were similarly observed for different metal oxides after ethanol exposure. 64-70 These species are formed when nucleophilic oxygen atoms from the surface of the catalyst attack the adsorbate. The presence of these acetate species suggests that ethanol is further oxidized when adsorbed on the surface of the catalyst, but only in a surface-bound state since no acetic acid was detected in the TPD. The lack of acetic acid formation can be explained by the weakly basic nature of MoO₃. The peaks at 1269 and 1624 cm⁻¹ in Figure 3A are characteristic of the enolate form of ethanol as shown in Scheme 2. Idriss and co-workers showed that ethanol forms a dihapto structure on the surface of ceria. 65,112 This suggests that the oxidation of ethanol results in the formation of an enolate that is more stable than acetaldehyde. The presence of the enolate indicates that a tautomerization mechanism readily occurs on the surface, and the enolate is stabilized by the surface. Interestingly, the enolate was also present on the oxidatively pretreated catalyst but not the R-MoO_x sample. This suggests that a certain amount of oxygen may be necessary on the surface to strongly bind the adsorbate in this dihapto configuration. As shown in the proposed mechanism (Scheme 2), the enolate is an intermediate for production of other species. Thus, its presence is needed for upgrading to chemicals other than acetaldehyde. It is also noteworthy to point out the tendency of ethanol to undergo dehydrogenation to ethoxide groups/aldehydes over all forms of the pretreated

The implications of this work for the field of sugar chemistry are significant. Simple organics with aldehyde and alcohol functionality were observed to behave differently over various pretreated versions of MoO₃. Sugars possess aldehyde, keto, and alcohol groups in rather complex molecules. For the simpler model compounds in the present study, it was shown that adsorption and condensation of these groups is greatly facilitated by CUS formed on MoO₃. In the work of Davis and

co-workers, Sn-BEA was shown to catalyze the isomerization of glucose to fructose but not the RAC of fructose to dihydroxyacetone and glyceraldehyde.⁷ However, MoO₃ was active for RAC, but had low activity for isomerization. When the solvent was switched from water to methanol, there was a significant increase in alkyl lactate yield, most likely due to defect sites created by the presence of the alcoholic solvent. The results shown here provide support for this finding by suggesting CUS of MoO_3 provide a specific environment with high catalytic activity for RAC sugars. A likely explanation for the stark differences in the reaction paths over Sn-BEA and MoO_x is the steric environment of the active sites in these materials. The Sn sites in Sn-BEA are in framework positions (i.e., zeolitic T-sites) with 4-fold coordination, and it is believed that one of the Sn-O-Si bonds is hydrolyzed to form the active "open" site, which should be a little more accessible. 113 This kind of domain lends itself to the formation of a sterically demanding cyclic transition state, in which two functional groups closely interact with the active site to enable a hydrogen transfer reaction. In contrast, Mo(VI) ions in the bulk of MoO₃ are 6-fold coordinated. While surface termination with Mo=O groups and the formation of defect sites will decrease this coordination number, the accessibility of the Mo site will remain much lower compared to LAS in Sn-BEA. Thus, the RAC reaction that only requires one aldehyde or keto group to interact with the LAS should be favored relative to a sterically more demanding isomerization reaction. The accessibility of the Mo site due to reduction is key, as it is possible for a sugar to undergo RAC in an oxygen containing environment, but only if it can interact with the site.¹¹ Another hypothesis is that CUS effectively stabilize the delocalization of the electron density of the carbonyl, thus leading to a more stable transition state. With this, oxygen atoms adjacent to the vacancy can become more nucleophilic and interact with alkoxide groups more strongly. Specifically, a bifunctional relationship on the surface of the catalyst is created where the CUS acts as an acid and a nearby nucleophilic oxygen becomes more basic. These effects allow the CUS to pull in the electrons of carbonyl oxygen atoms more strongly and the surface oxygen atom to stabilize the

adsorbate better. The propensity of MoO₃ to be reduced in alcoholic solvents, thus catalyzing RAC, hints at the extent of reduction of MoO₃ as a key descriptor for their performance.

5. CONCLUSIONS

This study has shown the role partial reduction of MoO₃ plays in the chemistry of simple oxygenates over MoO₃. Whereas thermal treatment of the catalyst in an inert environment led to partial reduction, treatment in H2 significantly increased the density of reduced sites. Partial reduction could also be achieved by pretreating the MoO3 with alcohols commonly used as solvents during (retro) aldol catalysis as shown by XPS and XANES. DFT-computed adsorption energies revealed that defects significantly favor the adsorption of oxygenates. The adsorption of aldehydes over CUS was more favored than alcohols. Furthermore, experimental DRIFTS and TPD studies showed that more reduced surfaces were far more active for (retro-)aldol coupling reactions. These results provide clear evidence of the importance of surface oxidation state on the catalytic activity and selectivity of MoO3 catalysts and suggest that catalytic activity can be tuned by solvent selection and/or catalyst pretreatment. The findings also highlight the importance of in situ or operando characterization of MoO₃ catalysts, particularly if operating in the presence of reducing solvents.

ASSOCIATED CONTENT

Supporting Information

The Supporting Information is available free of charge at https://pubs.acs.org/doi/10.1021/acscatal.0c01992.

XRD of MoO₃; XANES of methanol on MoO_x; digitized XANES spectra of MoO₃ and MoO₂; XPS of MoO₃; DFT adsorption geometries; DRIFTS of ethanol, acetaldehyde, and crotonaldehyde on MoO_x; vibrational frequencies; TPD molar desorption quantities; and images of MoO_x powder (PDF)

AUTHOR INFORMATION

Corresponding Authors

Andrew J. Medford — School of Chemical & Biomolecular Engineering and Renewable Bioproducts Institute, Georgia Institute of Technology, Atlanta, Georgia 30332, United States; Email: ajm@gatech.edu

J. Will Medlin – Department of Chemical and Biological Engineering, University of Colorado Boulder, Boulder, Colorado 80303, United States; Email: medlin@colorado.edu

Carsten Sievers — School of Chemical & Biomolecular Engineering and Renewable Bioproducts Institute, Georgia Institute of Technology, Atlanta, Georgia 30332, United States; orcid.org/0000-0002-5713-1875; Email: carsten.sievers@chbe.gatech.edu

Authors

Sean Najmi — School of Chemical & Biomolecular Engineering, Georgia Institute of Technology, Atlanta, Georgia 30332, United States

Mathew Rasmussen — Department of Chemical and Biological Engineering, University of Colorado Boulder, Boulder, Colorado 80303, United States

Giada Innocenti — School of Chemical & Biomolecular Engineering, Georgia Institute of Technology, Atlanta, Georgia 30332, United States; o orcid.org/0000-0003-2951-5457 Chaoyi Chang — School of Chemical & Biomolecular Engineering and Renewable Bioproducts Institute, Georgia Institute of Technology, Atlanta, Georgia 30332, United States

Eli Stavitski – National Synchrotron Light Source II, Brookhaven National Laboratory, Upton, New York 11973, United States

Simon R. Bare — Stanford Synchrotron Radiation Lightsource, SLAC National Accelerator Laboratory, Menlo Park, California 94025, United States

Complete contact information is available at: https://pubs.acs.org/10.1021/acscatal.0c01992

Author Contributions

*These authors contributed equally to this work.

Notes

The authors declare no competing financial interest.

ACKNOWLEDGMENTS

Financial support from the National Science Foundation (grant numbers: CBET-1705444/1705500) is gratefully acknowledged. S.N. is supported by the National Science Foundation Graduate Research Fellowship under Grant No. DGE-1650044. CC is supported by a Paper Science and Engineering Fellowship from the Renewable Bioproducts Institute at Georgia Tech. This research used beamline 7-BM (QAS) and 8-ID ISS (Inner Shell Spectroscopy) of the National Synchrotron Light Source II, a U.S. Department of Energy (DOE) Office of Science User Facility operated for the DOE Office of Science by Brookhaven National Laboratory under Contract No. DE-SC0012704. Use of the Stanford Synchrotron Radiation Lightsource, SLAC National Accelerator Laboratory, is supported by the U.S. Department of Energy, Office of Science, Office of Basic Energy Sciences under Contract No. DE-AC02-76SF00515. Co-ACCESS, is supported by the U.S. Department of Energy, Office of Science, Office of Basic Energy Sciences, Chemical Sciences, Geosciences and Biosciences. We thank Dr. Lu Ma for the help in collecting the XRD data, Dr. Adam Hoffman for his insight, experience, and assistance while running XAS measurements and Solumtochukwu Egboga for experimental support with IR studies.

REFERENCES

- (1) Huber, G. W.; Iborra, S.; Corma, A. Synthesis of Transportation Fuels from Biomass: Chemistry, Catalysts, and Engineering. *Chem. Rev.* **2006**, *106* (9), 4044–4098.
- (2) Corma, A.; Iborra, S.; Velty, A. Chemical Routes for the Transformation of Biomass into Chemicals. *Chem. Rev.* **2007**, *107* (6), 2411–2502.
- (3) Yue, H.; Zhao, Y.; Ma, X.; Gong, J. Ethylene Glycol: Properties, Synthesis, and Applications. *Chem. Soc. Rev.* **2012**, *41* (11), 4218–4244
- (4) Mäki-Arvela, P.; Simakova, I. L.; Salmi, T.; Murzin, D. Y. Production of Lactic Acid/Lactates from Biomass and Their Catalytic Transformations to Commodities. *Chem. Rev.* **2014**, *114* (3), 1909–1971
- (5) Caratzoulas, S.; Davis, M. E.; Gorte, R. J.; Gounder, R.; Lobo, R. F.; Nikolakis, V.; Sandler, S. I.; Snyder, M. A.; Tsapatsis, M.; Vlachos, D. G. Challenges of and Insights into Acid-Catalyzed Transformations of Sugars. *J. Phys. Chem. C* **2014**, *118* (40), 22815–22833.
- (6) Moliner, M.; Roman-Leshkov, Y.; Davis, M. E. Tin-Containing Zeolites Are Highly Active Catalysts for the Isomerization of Glucose in Water. *Proc. Natl. Acad. Sci. U. S. A.* **2010**, *107* (14), 6164–6168.

- (7) Orazov, M.; Davis, M. E. Tandem Catalysis for the Production of Alkyl Lactates from Ketohexoses at Moderate Temperatures. *Proc. Natl. Acad. Sci. U. S. A.* **2015**, *112* (38), 11777–11782.
- (8) Holm, M. S.; Saravanamurugan, S.; Taarning, E. Conversion of Sugars to Lactic Acid Derivatives Using Heterogeneous Zeotype Catalysts. *Science (Washington, DC, U. S.)* **2010**, 328 (5978), 602–605.
- (9) Pearson, R. G. Hard and Soft Acids and Bases. *J. Am. Chem. Soc.* 1963, 85 (22), 3533.
- (10) Suarez, W.; Dijmesic, J. A.; Hill, C. G. Acidic Properties of Molybdena-Alumina for Different Extents of Reduction: Infrared and Gravimetric Studies of Adsorbed Pyridine. *J. Catal.* **1985**, *94*, 408–421.
- (11) Brown, I. D.; Skowron, A. Electronegativity and Lewis Acid Strength. J. Am. Chem. Soc. 1990, 112 (9), 3401-3403.
- (12) Román-Leshkov, Y.; Moliner, M.; Labinger, J. A.; Davis, M. E. Mechanism of Glucose Isomerization Using a Solid Lewis Acid Catalyst in Waterok O.F. *Angew. Chem., Int. Ed.* **2010**, 49 (47), 8954–8957.
- (13) Rellán-Piñeiro, M.; López, N. The Active Molybdenum Oxide Phase in the Methanol Oxidation to Formaldehyde (Formox Process): A DFT Study. *ChemSusChem* **2015**, 8 (13), 2231–2239.
- (14) Miliordos, E.; Caratzoulas, S.; Vlachos, D. G. A Periodic-DFT Study of Retro-Aldol Fragmentation of Fuctose on MoO3. *Appl. Catal., A* **2017**, 530, 75–82.
- (15) Rellan-Pineiro, M.; Garcia-Ratés, M.; Lopez, N. Mechanism for the Selective Epimerization of the Glucose Mannose Pair by Mo-Based Compounds: Towards Catalyst Optimization. *Green Chem.* **2017**, *19*, 5932–5939.
- (16) Vohra, M.; Manwar, J.; Manmode, R.; Padgilwar, S.; Patil, S. Bioethanol Production: Feedstock and Current Technologies. *J. Environ. Chem. Eng.* **2014**, 2 (1), 573–584.
- (17) Silveira, M. H. L.; Morais, A. R. C.; Da Costa Lopes, A. M.; Olekszyszen, D. N.; Bogel-Łukasik, R.; Andreaus, J.; Pereira Ramos, L. Current Pretreatment Technologies for the Development of Cellulosic Ethanol and Biorefineries. *ChemSusChem* **2015**, 8 (20), 3366–3390.
- (18) Posada, J. A.; Patel, A. D.; Roes, A.; Blok, K.; Faaij, A. P. C.; Patel, M. K. Potential of Bioethanol as a Chemical Building Block for Biorefineries: Preliminary Sustainability Assessment of 12 Bioethanol-Based Products. *Bioresour. Technol.* **2013**, *135*, 490–499.
- (19) Barteau, M. A. Organic Reactions at Well-Defined Oxide Surfaces. Chem. Rev. 1996, 96 (4), 1413–1430.
- (20) Corson, B. B.; Jones, H. E.; Welling, C. E.; Hinckley, J. A.; Stahly, E. E. Butadiene from Ethyl Alcohol. Catalysis in the One-and Two-Stop Processes. *Ind. Eng. Chem.* **1950**, 42 (2), 359–373.
- (21) Ochoa, J. V.; Bandinelli, C.; Vozniuk, O.; Chieregato, A.; Malmusi, A.; Recchi, C.; Cavani, F. An Analysis of the Chemical, Physical and Reactivity Features of MgO-SiO2catalysts for Butadiene Synthesis with the Lebedev Process. *Green Chem.* **2016**, *18* (6), 1653—1663.
- (22) Angelici, C.; Weckhuysen, B. M.; Bruijnincx, P. C. A. Chemocatalytic Conversion of Ethanol into Butadiene and Other Bulk Chemicals. *ChemSusChem* **2013**, *6* (9), 1595–1614.
- (23) Chieregato, A.; Ochoa, J. V.; Bandinelli, C.; Fornasari, G.; Cavani, F.; Mella, M. On the Chemistry of Ethanol on Basic Oxides: Revising Mechanisms and Intermediates in the Lebedev and Guerbet Reactions. *ChemSusChem* **2015**, *8* (2), 377–388.
- (24) Sun, Z.; Vasconcelos, A. C.; Bottari, G.; Stuart, M. C. A.; Bonura, G.; Cannilla, C.; Frusteri, F.; Barta, K. Efficient Catalytic Conversion of Ethanol to 1-Butanol via the Guerbet Reaction over Copper- and Nickel-Doped Porous. *ACS Sustainable Chem. Eng.* **2017**, 5 (2), 1738–1746.
- (25) Toussaint, W. J.; Dunn, J. T.; Jachson, D. R. Production of Butadiene from Alcohol. *Ind. Eng. Chem.* 1947, 39 (2), 120–125.
- (26) Brunauer, S.; Emmett, P. H.; Teller, E. Adsorption of Gases in Multimolecular Layers. J. Am. Chem. Soc. 1938, 60 (2), 309–319.
- (27) Bolin, T. B.; Wu, T.; Schweitzer, N.; Lobo-Lapidus, R.; Kropf, A. J.; Wang, H.; Hu, Y.; Miller, J. T.; Heald, S. M. In Situ

- Intermediate-Energy X-Ray Catalysis Research at the Advanced Photon Source Beamline 9-BM. Catal. Today 2013, 205, 141–147.
- (28) Ravel, B.; Newville, M. Synchrotron Radiation ATHENA, ARTEMIS, HEPHAESTUS: Data Analysis for X-Ray Absorption Spectroscopy Using IFEFFIT. *J. Synchrotron Radiat.* **2005**, *12*, 537–541.
- (29) Baltrusaitis, J.; Mendoza-Sanchez, B.; Fernandez, V.; Veenstra, R.; Dukstiene, N.; Roberts, A.; Fairley, N. Generalized Molybdenum Oxide Surface Chemical State XPS Determination via Informed Amorphous Sample Model. *Appl. Surf. Sci.* **2015**, 326, 151–161.
- (30) Giannozzi, P.; Baroni, S.; Bonini, N.; Calandra, M.; Car, R.; Cavazzoni, C.; Ceresoli, D.; Chiarotti, G. L.; Cococcioni, M.; Dabo, I.; Dal Corso, A.; De Gironcoli, S.; Fabris, S.; Fratesi, G.; Gebauer, R.; Gerstmann, U.; Gougoussis, C.; Kokalj, A.; Lazzeri, M.; Martin-Samos, L.; Marzari, N.; Mauri, F.; Mazzarello, R.; Paolini, S.; Pasquarello, A.; Paulatto, L.; Sbraccia, C.; Scandolo, S.; Sclauzero, G.; Seitsonen, A. P.; Smogunov, A.; Umari, P.; Wentzcovitch, R. M. QUANTUM ESPRESSO: A Modular and Open-Source Software Project for Quantum Simulations of Materials. *J. Phys.: Condens. Matter* 2009, 21 (39), 395502.
- (31) Wellendorff, J.; Lundgaard, K. T.; Møgelhøj, A.; Petzold, V.; Landis, D. D.; Nørskov, J. K.; Bligaard, T.; Jacobsen, K. W. Density Functionals for Surface Science: Exchange-Correlation Model Development with Bayesian Error Estimation. *Phys. Rev. B: Condens. Matter Mater. Phys.* **2012**, 85 (23), 32–34.
- (32) Rellán-Piñeiro, M.; López, N. A Coupled Density Functional Theory-Microkinetic Modeling for the Hydrodeoxygenation of Glycerol to Propylene on MoO3. ACS Sustainable Chem. Eng. 2018, 6 (12), 16169–16178.
- (33) Coquet, R.; Willock, D. J. The (010) Surface of a-MoO3, a DFT + U Study. *Phys. Chem. Chem. Phys.* **2005**, 7 (22), 3819–3828.
- (34) Rellán-Piñeiro, M.; Lopez, N. One Oxygen Vacancy, Two Charge States: Characterization of Reduced α MoO 3 (010) through Theoretical Methods. *J. Phys. Chem. Lett.* **2018**, 9 (10), 2568–2573.
- (35) Pack, J. D.; Monkhorst, H. J. special Points for Brillouin-Zone Integrations"-a Reply. *Phys. Rev. B* **1977**, *16* (4), 1748–1749.
- (36) Bengtsson, L. Dipole Correction for Surface Supercell Calculations. *Phys. Rev. B: Condens. Matter Mater. Phys.* **1999**, 59 (19), 12301–12304.
- (37) Bahn, S. R.; Jacobsen, K. W. An Object-Oriented Scripting Interface to a Legacy Electronic Structure Code. *Comput. Sci. Eng.* **2002**, *4* (3), 56–66.
- (38) Brogaard, R. Y.; Henry, R.; Schuurman, Y.; Medford, A. J.; Moses, P. G.; Beato, P.; Svelle, S.; Nørskov, J. K.; Olsbye, U. Methanol-to-Hydrocarbons Conversion: The Alkene Methylation Pathway. *J. Catal.* **2014**, *314*, 159–169.
- (39) Delporte, P.; Meunier, F.; Pham-Huu, C.; Vennegues, P.; Ledoux, M. J.; Guille, J. Physical Characterization of Molybdenum Oxycarbide Catalyst; TEM, XRD and XPS. *Catal. Today* **1995**, 23 (3), 251–267.
- (40) Stiefel, E. I. Molybdenum Compounds. In *Kirk-Othmer Encyclopedia of Chemical Technology*; John Wiley & Sons, Inc.: Hoboken, NJ, 2011; pp 1-24 DOI: 10.1002/0471238961.1315122519200905.a01.pub3.
- (41) Kashiwabara, T.; Takahashi, Y.; Tanimizu, M.; Usui, A. Molecular-Scale Mechanisms of Distribution and Isotopic Fractionation of Molybdenum between Seawater and Ferromanganese Oxides. *Geochim. Cosmochim. Acta* **2011**, *75* (19), 5762–5784.
- (42) Lede, E. J.; Requejo, F. G.; Pawelec, B.; Fierro, J. L. G. XANES Mo L-Edges and XPS Study of Mo Loaded in HY Zeolite. *J. Phys. Chem. B* **2002**, *106* (32), 7824–7831.
- (43) Evans, J.; Frederick, J.; Mosselmans, W. L-Edge Studies on Molybdenum. *J. Phys. Chem.* **1991**, *95* (24), 9673–9676.
- (44) Aritani, H.; Tanaka, T.; Funabiki, T.; Yoshida, S.; Eda, K.; Sotani, N.; Kudo, M.; Hasegawa, S. Study of the Local Structure of Molybdenum-Magnesium Binary Oxides by Means of Mo L3-Edge XANES and UV-Vis Spectroscopy. *J. Phys. Chem.* **1996**, *100* (50), 19495–19501.

- (45) Bare, S. R. Surface Structure of Highly Dispersed MoO 3 on MgO Using in Situ Mo L 3-Edge XANES †. *Langmuir* 1998, 14, 1500–1504.
- (46) George, G. N.; Cleland, W. E.; Enemark, J. H.; Kipke, C. A.; Roberts, S. A.; Smith, B. E.; Cramer, S. P. L-Edge Spectroscopy of Molybdenum Compounds and Enzyme. *J. Am. Chem. Soc.* **1990**, *112* (7), 2541–2548.
- (47) Bare, S. R.; Mitchell, G. E.; Maj, J. J.; Vrieland, G. E.; Gland, J. L. Local Site Symmetry of Dispersed Molybdenum Oxide Catalysts: XANES at the Mo L2,3-Edges. *J. Phys. Chem.* **1993**, *97* (22), 6048–6053.
- (48) De Groot, F. M. F.; Hu, Z. W.; Lopez, M. F.; Kaindl, G.; Guillot, F.; Tronc, M. Differences between L3 and L2 X-Ray Absorption Spectra of Transition Metal Compounds. *J. Chem. Phys.* **1994**, *101* (8), 6570–6576.
- (49) Choy, J. H.; Kim, D. K.; Demazeau, G.; Jung, D. Y. LIII-Edge XANES Study on Unusually High Valent Iridium in a Perovskite Lattice. *J. Phys. Chem.* **1994**, *98* (25), *6258–6262*.
- (50) Cramer, S. P.; Eccles, T. K.; Kutzler, F. W.; Hodgson, K. O.; Mortenson, L. E. Molybdenum X-Ray Absorption Edge Spectra. The Chemical State of Molybdenum in Nitrogenase. *J. Am. Chem. Soc.* 1976, 98 (5), 1287–1288.
- (51) Wong, J.; Lytle, F. W.; Messmer, R. P.; Maylotte, D. H. K-Edge Absorption Spectra of Selected Vanadium Compounds. *Phys. Rev. B: Condens. Matter Mater. Phys.* **1984**, *30* (10), 5596–5610.
- (52) Asakura, H.; Shishido, T.; Yamazoe, S.; Teramura, K.; Tanaka, T. Structural Analysis of Group V, VI, and VII Metal Compounds by XAFS. J. Phys. Chem. C 2011, 115 (48), 23653–23663.
- (53) Yamamoto, T. Assignment of Pre-Edge Peaks in K-Edge x-Ray Absorption Spectra of 3d Transition Metal Compounds: Electric Dipole or Quadrupole? *X-Ray Spectrometry*. John Wiley and Sons, Ltd.; November 2008; pp 572–584 DOI: 10.1002/xrs.1103.
- (54) De Groot, F. M. F.; Hu, Z. W.; Lopez, M. F.; Kaindl, G.; Guillot, F.; Tronc, M. Differences between L3 and L2 X-Ray Absorption Spectra of Transition Metal Compounds. *J. Chem. Phys.* **1994**, *101* (8), 6570–6576.
- (55) Lede, E. J.; Requejo, F. G.; Pawelec, B.; Fierro, J. L. G. XANES Mo L-Edges and XPS Study of Mo Loaded in HY Zeolite. *J. Phys. Chem. B* **2002**, *106* (32), 7824–7831.
- (56) Nakamura, K.; Eda, K.; Sotani, N. Heat Treatment of Hydrogen Molybdenum Bronze in an Oxygen-Free Atmosphere. Formation of a Defect Structure and Attempt to Carry Out a Catalytic Reaction. *Bull. Chem. Soc. Jpn.* **1998**, *71* (9), 2063–2070.
- (57) Ressler, T.; Jentoft, R. E.; Wienold, J.; Günter, M. M.; Timpe, O. In Situ XAS and XRD Studies on the Formation of Mo Suboxides during Reduction of MoO3. *J. Phys. Chem. B* **2000**, *104* (27), 6360–6370.
- (58) Lv, M.; Xie, W.; Sun, S.; Wu, G.; Zheng, L.; Chu, S.; Gao, C.; Bao, J. Activated-Carbon-Supported K-Co-Mo Catalysts for Synthesis of Higher Alcohols from Syngas. *Catal. Sci. Technol.* **2015**, 5 (5), 2925–2934.
- (59) Choi, J. G.; Thompson, L. T. XPS Study of As-Prepared and Reduced Molybdenum Oxides. *Appl. Surf. Sci.* **1996**, 93 (2), 143–149
- (60) Bronkema, J. L.; Bell, A. T. Mechanistic Studies of Methanol Oxidation to Formaldehyde on Isolated Vanadate Sites Supported on High Surface Area Zirconia. *J. Phys. Chem. C* **2008**, *112* (16), 6404–6412
- (61) Araña, J.; Garriga I Cabo, C.; Doña-Rodríguez, J. M.; González-Díaz, O.; Herrera-Melián, J. A.; Pérez-Peña, J. FTIR Study of Formic Acid Interaction with TiO 2 and TiO 2 Doped with Pd and Cu in Photocatalytic Processes. *Appl. Surf. Sci.* **2004**, 239 (1), 60–71.
- (62) Kilos, B.; Bell, A. T.; Iglesia, E. Mechanism and Site Requirements for Ethanol Oxidation on Vanadium Oxide Domains. *J. Phys. Chem. C* **2009**, *113*, 2830–2836.
- (63) Del Arco, M.; Carriazo, D.; Gutiérrez, S.; Martín, C.; Rives, V. An FT-IR Study of the Adsorption and Reactivity of Ethanol on Systems Derived from Mg2Al-W7O246- Layered Double Hydroxides. *Phys. Chem. Chem. Phys.* **2004**, *6* (2), 465–470.

- (64) Appel, L. G.; Silva, C. G.; Zonetti, P. C.; Rodrigues, C. P.; Gaspar, A. B. Chemicals from Ethanol—The Acetone One-Pot Synthesis. *Appl. Catal., A* **2013**, 458, 111–118.
- (65) Yee, A.; Morrison, S. J.; Idriss, H. A Study of the Reactions of Ethanol on CeO 2 and Pd/CeO 2 by Steady State Reactions, Temperature Programmed Desorption, and In Situ FT-IR. *J. Catal.* **1999**, *186*, 279–295.
- (66) Madhavaram, H.; Idriss, H. Acetaldehyde Reactions over the Uranium Oxide System. J. Catal. 2004, 224 (2), 358–369.
- (67) Vohs, J. M.; Barteau, M. A. DEHYDRATION AND DEHYDROGENATION OF ETHANOL AND 1-PROPANOL ON THE POLAR SURFACES OF ZINC OXIDE. *Surf. Sci.* **1989**, 221, 590–608.
- (68) Kaichev, V. V.; Chesalov, Y. A.; Saraev, A. A.; Klyushin, A. Y.; Knop-Gericke, A.; Andrushkevich, T. V.; Bukhtiyarov, V. I. Redox Mechanism for Selective Oxidation of Ethanol over Monolayer V 2 O 5/TiO 2 Catalysts. *J. Catal.* **2016**, 338, 82–93.
- (69) Golay, S.; Doepper, R.; Renken, A. In-Situ Characterisation of the Surface Intermediates for the Ethanol Dehydration Reaction over g -Alumina under Dynamic Conditions. *Appl. Catal., A* **1998**, *172*, 97–106.
- (70) Yu, Z.; Chuang, S. S. C. In Situ IR Study of Adsorbed Species and Photogenerated Electrons during Photocatalytic Oxidation of Ethanol on TiO 2. *J. Catal.* **2007**, *246*, 118–126.
- (71) Foo, G. S.; Wei, D.; Sholl, D. S.; Sievers, C. Role of Lewis and Brønsted Acid Sites in the Dehydration of Glycerol over Niobia. *ACS Catal.* **2014**, *4*, 3180–3192.
- (72) Jentoft, J. C.; Schmelz, H.; Knozinger, H. Preparation of Selective Catalytic Reduction Catalysts via Milling and Thermal Spreading. *Appl. Catal., A* 1997, *161*, 167–182.
- (73) Vuurman, M. A.; Stufkens, D. J.; Oskam, A.; Deo, G.; Wachs, I. E. Combined Raman and IR Study of MOx-V2O5/Al2O3(MOx=MoO3, WO3, NiO, CoO) Catalysts under Dehydrated Conditions. *J. Chem. Soc., Faraday Trans.* **1996**, 92 (17), 3259–3265.
- (74) Rasko, J.; Kiss, J. Adsorption and Surface Reactions of Acetaldehyde. *Appl. Catal., A* **2005**, 287, 252–260.
- (75) Lochar, V.; Drobná, H. FTIR Study of the Interaction of Crotonaldehyde and Maleic Anhydride with V 2 O 5 and MoO 3. *Appl. Catal., A* **2004**, 269, 27–31.
- (76) De Jesús, J. C.; Zaera, F. Adsorption and Thermal Chemistry of Acrolein and Crotonaldehyde on Pt(111) Surfaces. *Surf. Sci.* **1999**, 430 (1), 99–115.
- (77) Zhu, L.; Lu, J. Q.; Chen, P.; Hong, X.; Xie, G. Q.; Hu, G. S.; Luo, M. F. A Comparative Study on Pt/CeO 2 and Pt/ZrO 2 Catalysts for Crotonaldehyde Hydrogenation. *J. Mol. Catal. A: Chem.* **2012**, 361–362, 52–57.
- (78) Englisch, M.; Jentys, A.; Lercher, J. A. Structure Sensitivity of the Hydrogenation of Crotonaldehyde over Pt/SiO2 and Pt/TiO2. *J. Catal.* **1997**, *166* (1), 25–35.
- (79) Xu, J.; Wu, P.; Ye, E. C.; Yuan, B. F.; Feng, Y. Q. Metal Oxides in Sample Pretreatment. TrAC. *TrAC*, *Trends Anal. Chem.* **2016**, 80, 41–56
- (80) Krishnankutty, N.; Vannice, M.A. The Effect of Pretreatment on Pd/C Catalysts: I. Adsorption and Absorption Properties. *J. Catal.* **1995**, *155*, 312–326.
- (81) Schimming, S. M.; Foo, G. S.; Lamont, O. D.; Rogers, A. K.; Yung, M. M.; D'Amico, A. D.; Sievers, C. Kinetics of Hydrogen Activation on Ceria-Zirconia. *J. Catal.* **2015**, *329*, 335–347.
- (82) Liang, Z.; Jiang, D.; Fang, G.; Leng, W.; Tu, P.; Tong, Y.; Liu, L.; Ni, J.; Li, X. Catalytic Enhancement of Aldol Condensation by Oxygen Vacancy on CeO 2 Catalysts. *ChemistrySelect* **2019**, *4* (14), 4364–4370.
- (83) Schaub, R.; Thostrup, P.; Lopez, N.; Lægsgaard, E.; Stensgaard, I.; Nørskov, J. K.; Besenbacher, F. Oxygen Vacancies as Active Sites for Water Dissociation on Rutile TiO2(110). *Phys. Rev. Lett.* **2001**, 87 (26), 266104–1–266104–4.
- (84) Puigdollers, A. R.; Schlexer, P.; Tosoni, S.; Pacchioni, G. Increasing Oxide Reducibility: The Role of Metal/Oxide Interfaces in

- the Formation of Oxygen Vacancies. ACS Catal. 2017, 7 (10), 6493–6513.
- (85) Xiao, X.; Bergstrom, H.; Saenger, R.; Johnson, B.; Sun, R.; Peterson, A. The Role of Oxygen Vacancies in Biomass Deoxygenation by Reducible Zinc/Zinc Oxide Catalysts. *Catal. Sci. Technol.* **2018**, *8* (7), 1819–1827.
- (86) Prasomsri, T.; Nimmanwudipong, T.; Román-Leshkov, Y. Effective Hydrodeoxygenation of Biomass-Derived Oxygenates into Unsaturated Hydrocarbons by MoO 3 Using Low H 2 Pressures. *Energy Environ. Sci.* **2013**, *6*, 1732–1738.
- (87) Schimming, S. M.; Lamont, O. D.; König, M.; Rogers, A. K.; D'Amico, A. D.; Yung, M. M.; Sievers, C. Hydrodeoxygenation of Guaiacol over Ceria-Zirconia Catalysts. *ChemSusChem* **2015**, 8 (12), 2073–2083.
- (88) Zhao, C.; Watt, C.; Kent, P. R.; Overbury, S. H.; Mullins, D. R.; Calaza, F. C.; Savara, A.; Xu, Y. Coupling of Acetaldehyde to Crotonaldehyde on CeO 2– x (111): Bifunctional Mechanism and Role of Oxygen Vacancies. *J. Phys. Chem. C* 2019, 123, 8273–8286.
- (89) Calaza, F. C.; Xu, Y.; Mullins, D. R.; Overbury, S. H. Oxygen Vacancy-Assisted Coupling and Enolization of Acetaldehyde on CeO2(111). *J. Am. Chem. Soc.* **2012**, *134* (43), 18034–18045.
- (90) Chu, D.; Zhao, C. Reduced Oxygen-Deficient CuWO4 with Ni Catalyzed Selective Hydrogenolysis of Cellulose to Ethylene Glycol. *Catal. Today* **2020**, *351*, 125–132.
- (91) Prasomsri, T.; Shetty, M.; Murugappan, K.; Roman-Leshkov, Y. Insights into the Catalytic Activity and Surface Modification of MoO 3 during the Hydrodeoxygenation of Lignin-Derived Model Compounds into Aromatic Hydrocarbons under Low Hydrogen Pressures. *Energy Environ. Sci.* **2014**, *7*, 2660–2669.
- (92) Nolte, M. W.; Zhang, J.; Shanks, B. H. Ex Situ Hydro-deoxygenation in Biomass Pyrolysis Using Molybdenum Oxide and Low Pressure Hydrogen. *Green Chem.* **2016**, *18* (1), 134–138.
- (93) Bligaard, T.; Nørskov, J. K.; Dahl, S.; Matthiesen, J.; Christensen, C. H.; Sehested, J. The Brønsted–Evans–Polanyi Relation and the Volcano Curve in Heterogeneous Catalysis. *J. Catal.* **2004**, 224, 206–217.
- (94) Medford, A. J.; Vojvodic, A.; Hummelshøj, J. S.; Voss, J.; Abild-Pedersen, F.; Studt, F.; Bligaard, T.; Nilsson, A.; Nørskov, J. K. From the Sabatier Principle to a Predictive Theory of Transition-Metal Heterogeneous Catalysis. *J. Catal.* **2015**, 328, 36–42.
- (95) Idriss, H.; Seebauer, E. G. Reactions of Ethanol over Metal Oxides. J. Mol. Catal. A: Chem. 2000, 152, 201-212.
- (96) Takezawa, N.; Hanamaki, C.; Kobayashi, H. The Mechanism of Dehydrogenation of Ethanol on Magnesium Oxide. *J. Catal.* **1975**, 38 (1–3), 101–109.
- (97) Mudiyanselage, K.; Al-Shankiti, I.; Foulis, A.; Llorca, J.; Idriss, H. Reactions of Ethanol over CeO2 and Ru/CeO2 Catalysts. *Appl. Catal., B* **2016**, *197*, 198–205.
- (98) Tatibouet, J. M.; German, J. E. A Structure-Sensitive Oxidation Reaction: Methanol on Molybdenum Trioxide Catalysts. *J. Catal.* **1981**, 72 (2), 375–378.
- (99) Oyama, S. T.; Zhang, W. True and Spectator Intermediates in Catalysis: The Case of Ethanol Oxidation on Molybdenum Oxide As Observed by in Situ Laser Raman Spectroscopy. *J. Am. Chem. Soc.* **1996**, *118*, 7173–7177.
- (100) Smith, R. L. The Structural Evolution of the MoO_3 (010) Surface during Reduction and Oxidation Reactions, 1998.
- (101) Zhang, W.; Desikan, A.; Oyama, S. T. Effect of Support in Ethanol Oxidation on Molybdenum Oxide. *J. Phys. Chem.* **1995**, *99* (39), 14468–14476.
- (102) Seman, M.; Kondo, J. N.; Domen, K.; Radhakrishnan, R.; Oyama, S. T. Reactive and Inert Surface Species Observed during Methanol Oxidation over Silica-Supported Molybdenum Oxide. *J. Phys. Chem. B* **2002**, *106* (50), 12965–12977.
- (103) Pomalaza, G.; Capron, M.; Ordomsky, V.; Dumeignil, F. Recent Breakthroughs in the Conversion of Ethanol to Butadiene. *Catalysts* **2016**, *6* (12), 203.
- (104) Sun, J.; Wang, Y. Recent Advances in Catalytic Conversion of Ethanol to Chemicals. ACS Catal. 2014, 4 (4), 1078–1090.

- (105) Jones, M. D. Catalytic Transformation of Ethanol into 1,3-Butadiene. *Chem. Cent. J.* **2014**, *8* (1), 1–5.
- (106) Kung, H. H. Chapter 4. Surface Coordinative Unsaturation. In *Transition Metal Oxides Surface Chemistry and Catalysis*; Delmon, B., Yates, J., Eds.; Elsevier Science Publishing Company Inc.: New York, NY, 1991; pp 53–71.
- (107) Mann, A. K. P.; Wu, Z.; Calaza, F. C.; Overbury, S. H. Adsorption and Reaction of Acetaldehyde on Shape-Controlled CeO2 Nanocrystals: Elucidation of Structure-Function Relationships. *ACS Catal.* **2014**, *4* (8), 2437–2448.
- (108) Chen, T. L.; Mullins, D. R. Adsorption and Reaction of Acetaldehyde over CeOX(111) Thin Films. *J. Phys. Chem. C* **2011**, 115 (8), 3385–3392.
- (109) Chong, S. V.; Idriss, H. Reactions of Acetaldehyde on UO2(111) Single Crystal Surfaces. Evidence of Benzene Formation. *J. Vac. Sci. Technol., A* **2001**, *19* (4), 1933–1937.
- (110) Wang, S.; Goulas, K.; Iglesia, E. Condensation and Esterification Reactions of Alkanals, Alkanones, and Alkanols on TiO2: Elementary Steps, Site Requirements, and Synergistic Effects of Bifunctional Strategies. *J. Catal.* **2016**, 340, 302–320.
- (111) Rekoske, J. E.; Barteau, M. A. Competition between Acetaldehyde and Crotonaldehyde during Adsorption and Reaction on Anatase and Rutile Titanium Dioxide. *Langmuir* **1999**, *15* (6), 2061–2070.
- (112) Idriss, H.; Diagne, C.; Hindermann, J. P.; Kiennemann, A.; Barteau, M. A. Reactions of Acetaldehyde on CeO2 and CeO2-Supported Catalysts. *J. Catal.* **1995**, *155*, 219–237.
- (113) Bermejo-Deval, R.; Assary, R. S.; Nikolla, E.; Moliner, M.; Roman-Leshkov, Y.; Hwang, S.-J.; Palsdottir, A.; Silverman, D.; Lobo, R. F.; Curtiss, L. A.; Davis, M. E. Metalloenzyme-like Catalyzed Isomerizations of Sugars by Lewis Acid Zeolites. *Proc. Natl. Acad. Sci. U. S. A.* **2012**, *109* (25), 9727–9732.
- (114) Zhang, J.; Liu, X.; Sun, M.; Ma, X.; Han, Y. Direct Conversion of Cellulose to Glycolic Acid with a Phosphomolybdic Acid Catalyst in a Water Medium. *ACS Catal.* **2012**, *2* (8), 1698–1702.